

A Click Chemistry Strategy for the Synthesis of Efficient Photoinitiators for Two-Photon Polymerization

Irene Henning, Adam W. Woodward, Graham A. Rance, Benjamin T. Paul, Ricky D. Wildman, Derek J. Irvine, and Jonathan C. Moore*

It is reported that efficient photoinitiators, suitable for two-photon polymerization, can be obtained using the copper catalyzed azide/alkyne cycloaddition reaction. This click chemistry strategy provides a modular approach to the assembly of photoinitiators that enables the rapid variation of key fragments to produce photoinitiators with desirable properties. To assess the performance of the first-in-class photoinitiators generated by this approach, a screening method is developed to enable the rapid determination of polymerization and damage thresholds in numerous photoresists during two-photon polymerization. The degree of consumption of vinyl groups (DC) and homogeneity of the polymerization are further assessed by micro-Raman spectroscopy. Finally, more complex structures are fabricated to demonstrate that the efficient two-photon polymerization of stable 3D microarchitectures can be achieved using triazole-based photoinitiators.

1. Introduction

The accurate fabrication of micro- and nanoscale objects of predefined geometry is key to the further progression of a diverse range of fields including micro-optics,^[1] electronics,^[2] biomedicine,^[3] microfluidics,^[4] and microelectromechanical systems.^[5] Two-photon polymerization is the most precise 3D printing technique, enabling feature sizes below the diffraction limit of light (<100 nm).^[2] This approach hinges on the application of photoinitiators that are able to simultaneously absorb two photons (each with half the energy of the spectral-gap) in order to reach an excited state. Unlike single-photon absorption, two-photon absorption has a nonlinear dependence on light intensity, making it possible to

localize photochemically induced polymerization to the focal point of a laser beam that has been passed through a microscope objective.^[6] It is well established that a key factor in determining many important properties of the printing process, such as feature size and fabrication time, is the efficiency of the photoinitiator.^[2,7] Despite their importance, the development of two-photon absorbing photoinitiators has been much slower than that of their classical UV counterparts, which have been widely commercialized. This is due, in part, to limited academic research, which has been impeded by the lengthy synthetic sequences that are typically employed for generation of the required planar π -systems. This has been highlighted as a critical obstruction to the further advancement of two-photon polymerization.^[8] It is well established that the most successful motifs for two-photon absorbing materials comprise electron donating and accepting functionalities, separated by π -bridges, in various configurations (A- π -B, A- π -B- π -A, B- π -A- π -B, etc.).^[9] The identity and arrangement of these fragments determines the photophysical and chemical properties of the photoinitiator and subsequently, its suitability for different applications.^[10,11] We surmised that a general and straightforward method to couple these key fragments would constitute a useful method for the synthesis of two-photon-absorbing photoinitiators that would overcome the synthetic shortcomings mentioned above. Such an approach could provide a useful tool for the rapid development of new photoinitiators to meet specific and bespoke applications. To achieve these ends, we would require a robust and reliable method for chemical ligation, features


Dr. I. Henning, Dr. B. T. Paul, Prof. R. D. Wildman, Prof. D. J. Irvine
Center for Additive Manufacturing
Faculty of Engineering
University of Nottingham
Jubilee Campus, Nottingham NG7 2RD, UK

Dr. A. W. Woodward
School of Chemistry
University of Manchester
Oxford Road, Manchester M13 9PL, UK

Dr. A. W. Woodward
Photon Science Institute
University of Manchester
Oxford Road, Manchester M13 9PL, UK

Dr. G. A. Rance
Nanoscale and Microscale Research Centre (nmRC)
University of Nottingham
University Park
Nottingham NG7 2RD, UK

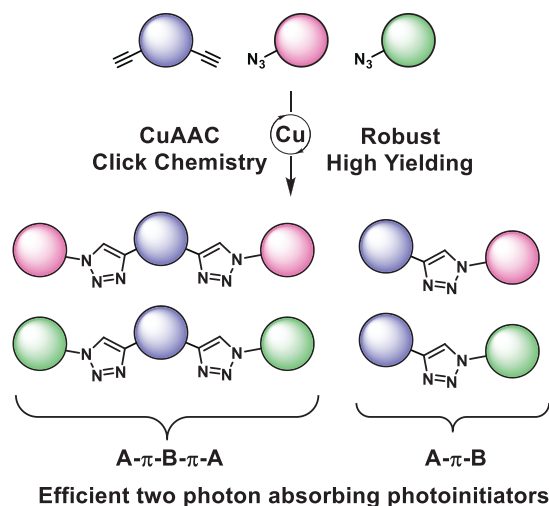
Dr. G. A. Rance, Dr. J. C. Moore
School of Chemistry
University of Nottingham
University Park, Nottingham NG7 2RD, UK
E-mail: pczjm@nottingham.ac.uk

 The ORCID identification number(s) for the author(s) of this article can be found under <https://doi.org/10.1002/adfm.202006108>.

© 2020 The Authors. Published by Wiley-VCH GmbH. This is an open access article under the terms of the Creative Commons Attribution License, which permits use, distribution and reproduction in any medium, provided the original work is properly cited.

DOI: 10.1002/adfm.202006108

This study:



Scheme 1. Click chemistry-enabled synthesis of A-π-B-π-A and A-π-B photoinitiators for two-photon polymerization.

that are commonly associated with the copper catalyzed azide/alkyne cycloaddition (CuAAC) reaction. This reaction has become almost synonymous with the concept of “click chemistry”; a philosophy that aims to develop general, selective, and high yielding reactions to expedite chemical synthesis.^[12] The CuAAC reaction has seen wide-spread application in organic chemistry but also in materials science, bioconjugation, and many other fields.^[13,14] There is precedent for using the CuAAC reaction to generate various organic dyes and fluorophores,^[15a] including UV-photoinitiators^[15b] and fluorescent small molecules^[15c] and polymers^[15d] that display aggregation induced emission. Despite this, only a selection of these materials have been studied for multiphoton processes^[15e] and to the best of our knowledge, the CuAAC reaction has never been employed for the synthesis of photoinitiators for two-photon polymerization.

Our strategy was to generate alkyne and azido functionalized derivatives of known donor and acceptor units and append these fragments using CuAAC click chemistry (Scheme 1). This approach would allow systematic variations in structure that could be explored to understand the key relationships governing behavior. The resultant triazole-based photoinitiators were studied both in terms of their photophysical properties and for their ability to facilitate efficient two-photon polymerization with micro- and nanometer feature size. Due to microscopic reaction volumes and fast reaction times, two-photon polymerization kinetics are generally challenging to study.^[16] Thus, a screening assay was developed to expedite the evaluation of 30 photoresist compositions that were used for the micro-fabrication of 3D architectures. A selection of these structures were then further analyzed by micro-Raman spectroscopy to establish the degree of consumption of vinyl groups (DC) and the homogeneity of the polymerization. Finally, a series of bucky ball-type domes were fabricated to demonstrate that the efficient two-photon polymerization of stable 3D microarchitectures can be achieved using this new class of click chemistry-enabled photoinitiators.

2. Results and Discussion

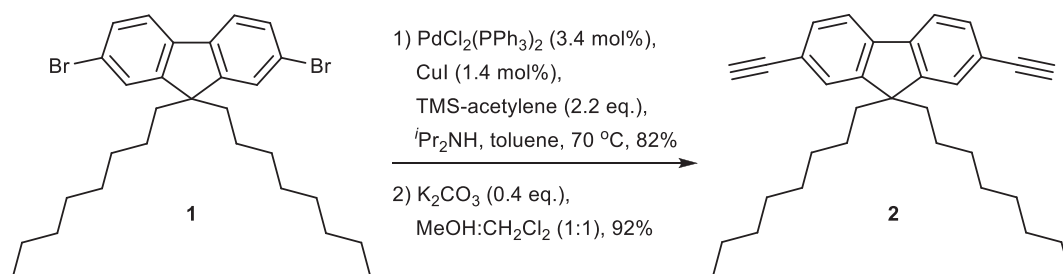
2.1. Photoinitiator Synthesis

Based on literature precedent for the design of two-photon absorbing photoinitiators, we selected the fluorene derivative **2** as the dialkynyl fragment and the *N,N*-dimethyl and -diphenyl phenylamines **7** and **8** as the azido components (Scheme 2).^[17] The fluorene moiety constitutes a thermally and photochemically stable analogue of biphenyl, where “locking” the aromatic rings with a central cyclopentyl unit serves to increase electron delocalization via increased π -orbital overlap.^[18] This in turn increases molecular polarizability. An added feature of the fluorene moiety is that the 9,9' position can be used to append further functionality, such as solubilizing groups, e.g., dioctyl chains. Fluorene derivatives have seen wide-spread application in a number of fields related to photonics including bioimaging,^[19–21] lasing,^[22,23] and two-photon microfabrication,^[24,25] where the motif has been used as both a central core^[26] and as a π -linker.^[27] Similarly, *N,N*-dialkyl and -diaryl phenylamines, such as **7** and **8** have also been widely employed in the design of photoinitiators, largely due to their strong electron donating abilities.^[10,28]

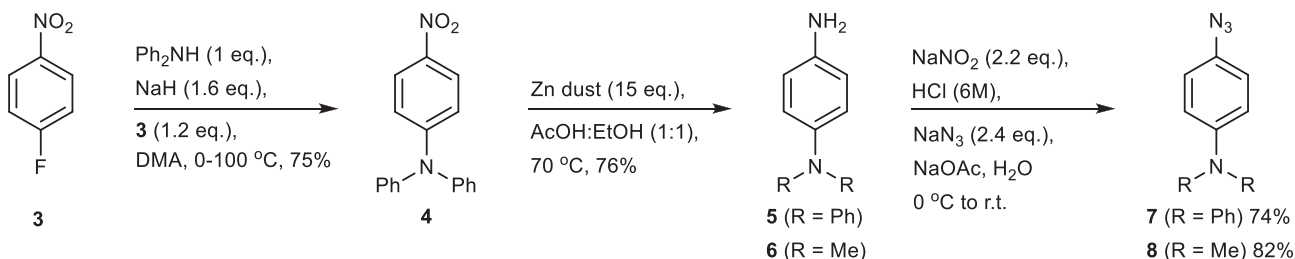
The targeted dialkynyl fluorene **2** was prepared in two-steps via a two-directional Sonogashira cross-coupling of the corresponding dibromo derivative **1** with trimethylsilyl acetylene^[29] followed by desilylation with potassium carbonate in methanol (Scheme 2). The azido coupling-partners **7** and **8** were obtained from the corresponding anilines via diazotization and displacement with sodium azide.^[30] In the case of the *N,N*-dimethyl derivative, the commercially available aniline **6** was employed, whereas the *N,N*-diphenyl aniline **5** was prepared in two-steps from 1-fluoro-4-nitrobenzene (**3**) via substitution with diphenylamine^[31] followed by a zinc-mediated nitro-reduction. With these precursors in hand, we proceeded to investigate conditions for the CuAAC click chemistry reaction, targeting the mono and bis-triazoles **Me-Mono**, **Ph-Mono**, **Me-Bis**, and **Ph-Bis** (Scheme 2).

Initially, we employed the classical procedure, namely $\text{Cu}(\text{SO}_4)_2$ as precatalyst and sodium ascorbate as reductant.^[32] At room temperature, the reaction of the diyne **2** and the azide **8** gave only a trace of the desired bis-triazole **Me-Bis** under these conditions (Table 1, Entry 1). When the reaction was repeated at 50 °C, **Me-Bis** was obtained in an improved yield of 64% alongside the unreacted diyne **2** (Table 1, Entry 2). Next, we investigated $\text{Cu}(\text{MeCN})_4\text{PF}_6$ as the catalyst, an organic-soluble and comparatively stable Cu(I) source that negates the need for a stoichiometric reductant.^[33] Pleasingly, with this catalyst the reaction proceeded at room temperature however a lower yield of **Me-Bis** was obtained, with the mono triazole **Me-Mono** being formed as the major product (Table 1, Entry 3). The optimal conditions were found when *tris*-(benzyltriazolylmethyl)amine (TBTA) was incorporated into the catalytic system (Table 1, Entry 4). This ligand's utility is proposed to be twofold; it accelerates catalysis by providing additional electron density to the metal center and concurrently stabilizes the catalytically active copper(I) species against oxidation to copper(II).^[34] Under these optimized conditions, near quantitative yields of the targeted photoinitiators **Me-Bis** and **Ph-Bis** could be obtained (96% and 99% yield, respectively) (Scheme 2). Furthermore, by simply changing the stoichiometry (2 equiv. of diyne, 1 equiv.

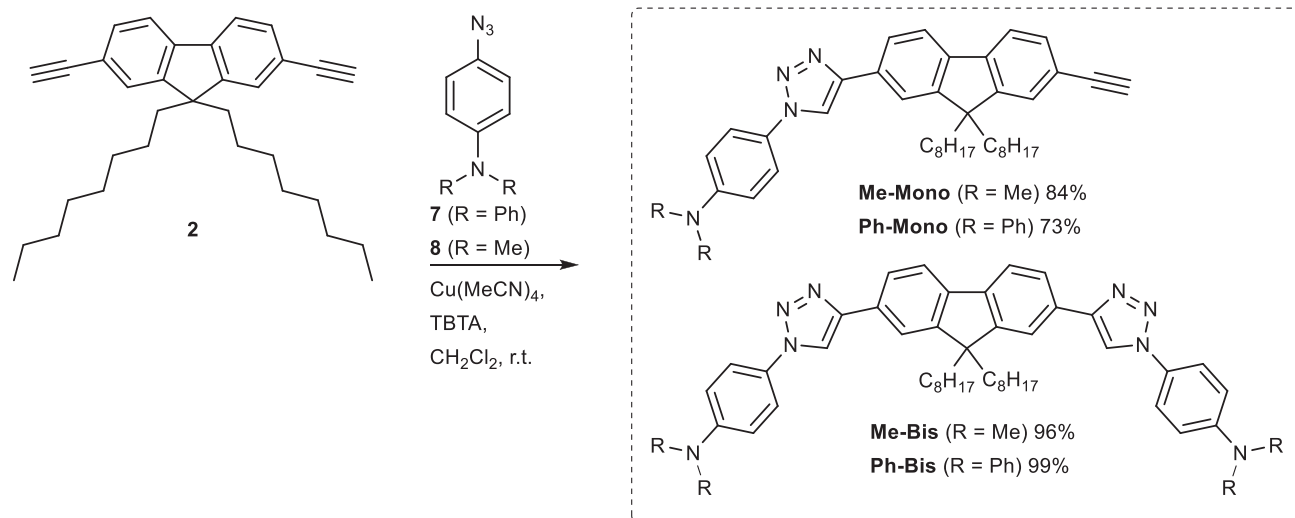
A - Synthesis of Dialkynyl CuAAC Precursor



B - Synthesis of Azido CuAAC Precursor



C - CuAAC-Mediated Synthesis of Two-Photon Absorbing Initiators



Scheme 2. Synthetic routes to the key photoinitiator precursors **2**, **7**, and **8** and their subsequent coupling via the CuAAC click chemistry reaction to form the targeted mono- and bis-triazole containing photoinitiators **Me-Mono**, **Ph-Mono**, **Me-Bis**, and **Ph-Bis**.

Table 1. Development of reaction conditions for the CuAAC click reaction. The reaction was optimized using the diyne **2** and the azide **8** as substrates.

Entry	2 + 8		Solvent	Temp.	Result
	(1 equiv.)	(2.1 equiv.)			
	Conditions (see table)				Me-Mono + Me-Bis
1	Cu(SO ₄) ₂	Sodium ascorbate	tBuOH:H ₂ O	r.t.	Trace
2	Cu(SO ₄) ₂	Sodium ascorbate	tBuOH:H ₂ O	50 °C	64% (Me-Bis)
3	Cu(MeCN) ₄ PF ₆	—	DCM	r.t.	19% (Me-Mono:Me-Bis =1.6:1)
4	Cu(MeCN) ₄ PF ₆	TBTA	DCM	r.t.	96% (Me-Bis)

Table 2. Photophysical data for the photoinitiators in toluene.

Photoinitiator	$\lambda_{\text{max}}^{\text{abs}}$ [nm]	$\lambda_{\text{max}}^{\text{em}}$ [nm]	$\Delta\lambda$ [nm] [(cm^{-1})]	Φ_f [%]	τ [ns]
Me-Mono	340	394	54 (4030)	50.8	0.96
Me-Bis	338	388	50 (3810)	63.0	0.92
Ph-Mono	343	390	47 (3510)	67.3	1.02
Ph-Bis	352	385	33 (2440)	58.3	0.84

azide), the corresponding mono-triazole products **Me-Mono** and **Ph-Mono** were also accessed in good yield. **Me-Mono** was obtained in 84% alongside 14% of **Me-Bis** (98% overall yield), whereas **Ph-Mono** was obtained in 73% yield alongside the recovered diyne **2** (Scheme 2).

2.2. Photophysical Measurements

Absorption, emission, and excitation spectra were recorded for the triazole-based initiators **Me-Mono**, **Ph-Mono**, **Me-Bis**, and **Ph-Bis** alongside fluorescence quantum yield and fluorescence lifetime measurements (Table 2; and Table S1, Supporting Information). The absorption spectra for the triazole-based initiators (Figure 1A, solid lines) show close agreement ($\lambda_{\text{max}}^{\text{abs}} \approx 340$ nm), with the exception of **Ph-Bis** ($\lambda_{\text{max}}^{\text{abs}} = 350$ nm) which was attributed to the two strong donor moieties feeding electrons into the π -system, increasing the effective conjugation and redshifting the energy of the electronic transition. The spectra for **Ph-Mono** and **Ph-Bis** display a pronounced shoulder at ≈ 300 nm as a result of this triphenylamine moiety. The emission spectra for these compounds (Figure 1A, dashed lines) display equal agreement ($\lambda_{\text{max}}^{\text{em}} \approx 390$ nm), indicating that the emission is coming from the same excited state. Each of the triazole-based initiators display comparable fluorescence quantum yields ($\Phi_f = 50.8$ – 67.3%), and fluorescence lifetimes ($\tau = 0.84$ – 1.02 ns) (Table 2).

Two-photon absorption cross sections were determined for the compounds using a relative method, comparing the two-photon

upconverted fluorescence of each sample to that of Rhodamine B (Figure 1B) as permitted by the tuning range of the Ti:sapphire laser.^[35] The absorption cross sections calculated for the *N,N*-diphenyl derivatives **Ph-Mono** and **Ph-Bis** were roughly double those of the *N,N*-dimethyl derivatives **Me-Mono** and **Me-Bis**. This is presumably a result of the diphenylamino moiety being a better electron donating group, allowing for a greater dipole shift upon excitation.^[36] It is well established that extended π -conjugation is a key contributor to the magnitude of a compound's two-photon cross section.^[9] Despite this, the bis-triazole species **Me-Bis** and **Ph-Bis** display equivalent two-photon cross sections to their respective mono-triazole analogues **Me-Mono** and **Ph-Mono**, respectively. This highlights that in this series, the functionality on the amino donor groups is a more significant factor in determining two-photon cross section than the extent of π -conjugation. This is likely due to the fact that these compounds lack a strong acceptor moiety to drive the movement of electron density between the ground and excited states.^[37–40]

2.3. Evaluation of the Initiators' Performance in Two-Photon Polymerization

Due to the complex sequence of photochemical and chemical events that are involved in two-photon polymerization, no individual photophysical parameter will display direct correlation to a compound's real-life performance as an initiator. For example, the two-photon cross-section (δ_{2PA}) is a key parameter but there are

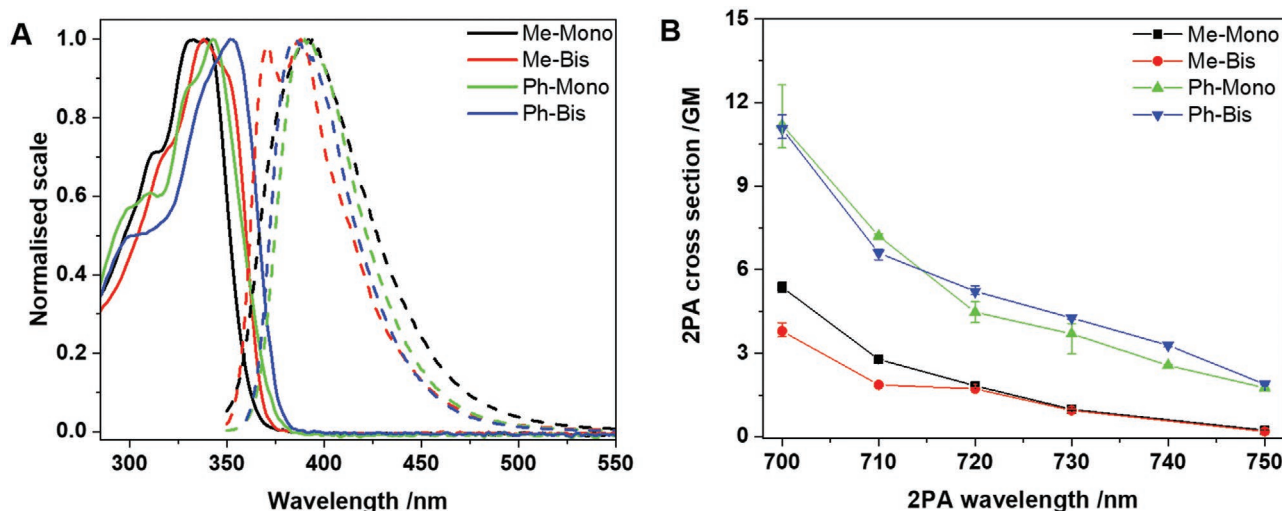


Figure 1. A) Absorption (solid line), and emission (dashed line) spectra and B) two-photon absorption spectra for photoinitiators **Me-Mono** (black), **Me-Bis** (red), **Ph-Mono** (green), **Ph-Bis** (blue), in toluene.

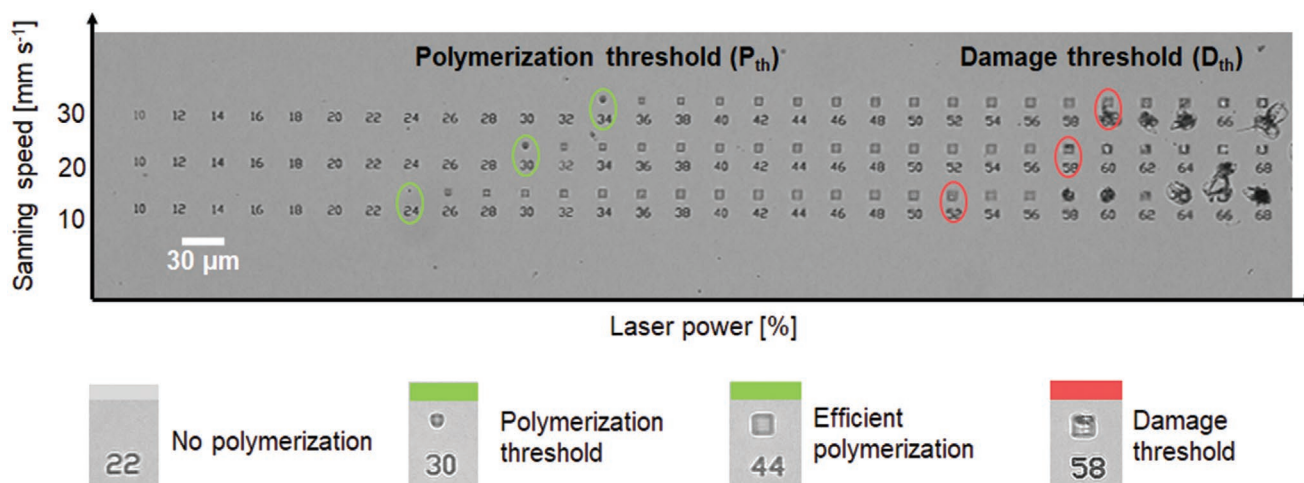


Figure 2. A bright-field image of an exemplar array of $5 \times 5 \times 5 \mu\text{m}$ cubes fabricated for the rapid determination of the polymerization- and damage thresholds (P_{th} and D_{th}) for each photoresist composition. Below is a close-up showing the visual determination of P_{th} and D_{th} . To enable quick assignment of the laser power used, each cube was fabricated with text printed below stating the percentage of the maximum laser power applied (10–100% laser power with 5% increments equivalent to 2 mW increments).

numerous examples where this value has been shown to correlate poorly with an initiator's performance in two-photon polymerization.^[25,41–44] The most direct method of assessing a candidate photoinitiator for two-photon polymerization is through the fabrication of a series of 3D-test structures.^[7,42] In this way, direct comparisons can be made between a series of candidate compounds in relation to a previously established photoinitiator.

For this study, polyethylene glycol diacrylate (PEGDA, Mn 700) and pentaerithrityl triacrylate (PETA) were selected as the monomers as they represent two of the simplest and most commonly employed di- and tri-acrylate systems, respectively, for two-photon lithography. The commonly employed and commercially available photoinitiator Irgacure369 (**I369**) was used as a reference compound.^[17,45,46] Arrays of $5 \times 5 \times 5 \mu\text{m}$ cubes were fabricated using three different photoinitiator concentrations ($0.8 \times 10^{-3} \text{ M}$, $4 \times 10^{-3} \text{ M}$, and $8 \times 10^{-3} \text{ M}$), while applying a range of laser powers (4–40 mW) and scanning speeds (10, 20, and 30 mm s^{-1}). It should be noted that these concentrations approximately equate to 0.1 wt%, 0.5 wt%, and 1 wt%, respectively. Following fabrication, the polymeric structures were imaged using bright field microscopy. This allowed rapid evaluation of the photoinitiators' performance through comparison of the polymerization and damage threshold powers (P_{th} and D_{th}) at a wide range of microfabrication parameters (**Figure 2**). P_{th} was defined as the laser power at which polymerized material could be observed^[47] and D_{th} was defined as the minimum laser power at which the destructive effects of heat formation became visible.^[48] The threshold values P_{th} and D_{th} determine the polymerization window, which is defined as the range of laser powers and scanning speeds that allow efficient two-photon polymerization. Wide polymerization windows are critical for high throughput in mass production^[49] and ensure reproducible results by buffering natural fluctuations in photoresist compositions.^[50] Using the described method, it was possible to rapidly assess the polymerization characteristics and determine the polymerization windows in 30 different photoresist compositions. All repeats exhibited low standard deviations ($\text{SD}_{\text{max}} = 0.8 \rightarrow$ coefficient of variation = 0.33).

Initially, P_{th} and D_{th} were determined at three different photoinitiator concentrations, using a laser scanning speed of 20 mm s^{-1} , and applying laser powers from 4 to 40 mW (**Figure 3A,B**). When using PEGDA as the monomer, we were pleased to observe that all four of the novel triazole-based initiators were found to be active for two-photon polymerization. Furthermore, **Me-Mono** and **Ph-Mono** displayed comparable processing windows to the commercial initiator **I369** with both PEGDA and PETA at $4 \times 10^{-3} \text{ M}$ and $8 \times 10^{-3} \text{ M}$ concentrations. Impressively, both **Me-Mono** and **Ph-Mono** were also active at $0.8 \times 10^{-3} \text{ M}$, whereas **I369** was completely inactive at this concentration. This is significant, as low photoinitiator concentrations are often desirable, particularly in biomedical applications due to the cytotoxicity and optical interferences caused by residual photoinitiator in the polymerized structures.^[51]

In PEGDA polymerizations, the results obtained with **Me-Mono** and **Ph-Mono** followed the expected trend, with P_{th} reducing as photoinitiator concentrations increased (**Figure 3A**).^[52] Specifically, as the initiator concentration was increased from $0.8 \times 10^{-3} \text{ M}$ to $4 \times 10^{-3} \text{ M}$, a decrease in P_{th} of 30% and 20% was observed for **Me-Mono** and **Ph-Mono**, respectively. A further increase in concentration from $4 \times 10^{-3} \text{ M}$ to $8 \times 10^{-3} \text{ M}$ led to smaller reductions in P_{th} of 8% and 6%, respectively. In comparison, with **I369** the P_{th} decreased by 20% when the concentration was increased from $4 \times 10^{-3} \text{ M}$ to $8 \times 10^{-3} \text{ M}$, which further demonstrates that the optimal concentration for **I369** is considerably higher than it is for the novel triazole-based initiators. Interestingly, when **Me-Bis** and **Ph-Bis** were evaluated with PEGDA, an increase in photoinitiator concentration from $4 \times 10^{-3} \text{ M}$ to $8 \times 10^{-3} \text{ M}$ led to increased P_{th} 's and D_{th} 's (**Figure 3A**). This was ascribed to solubility issues; at $8 \times 10^{-3} \text{ M}$ the photoresists containing **Me-Bis** and **Ph-Bis** (which were clear and colorless on preparation) were observed to become turbid after standing for prolonged periods, which indicates poor solubility at this concentration. Following precipitation, the true concentration of initiator in solution would of course be reduced, which is consistent with the observed increase in P_{th} and D_{th} (**Figure 3A**).

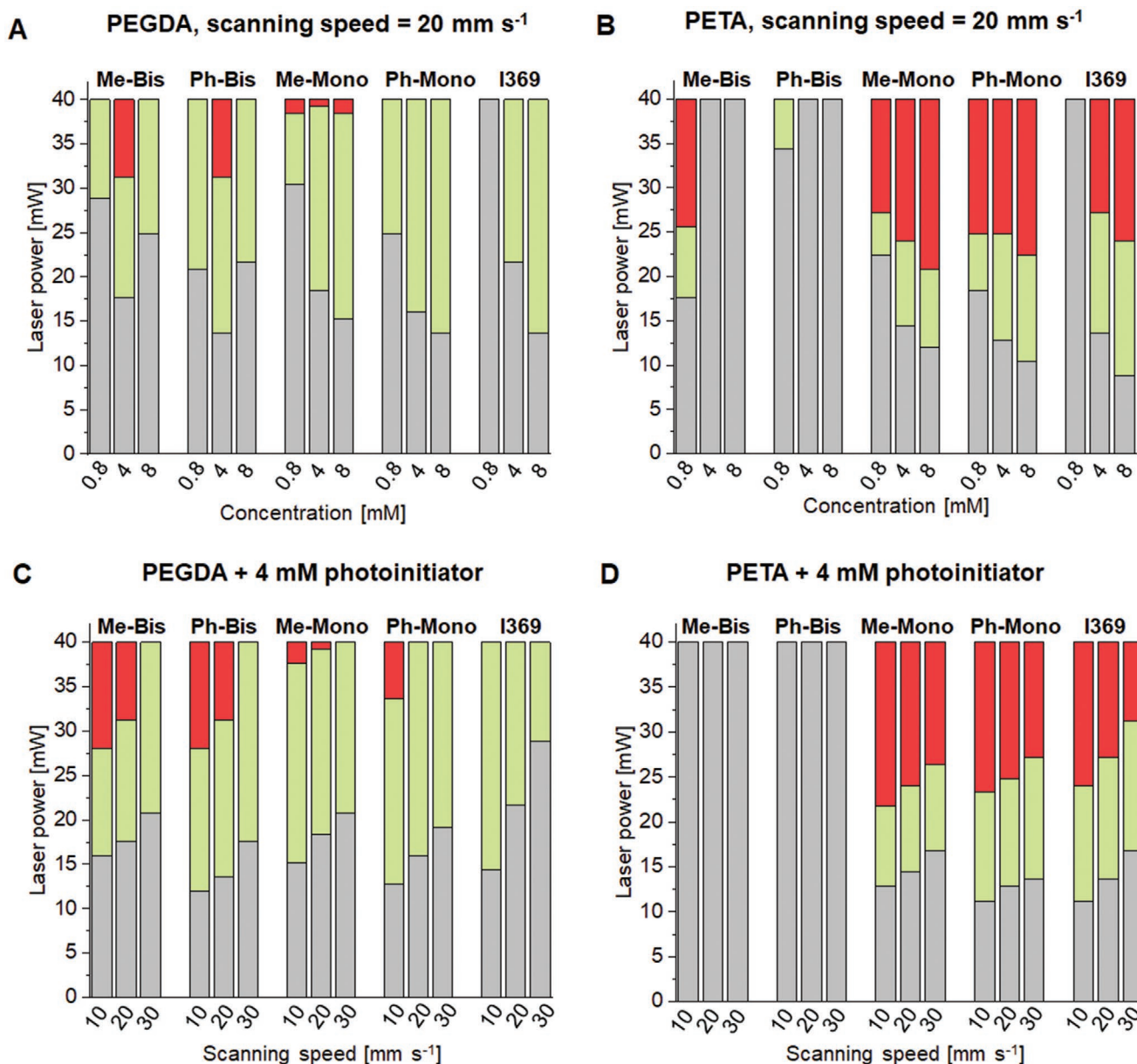


Figure 3. Comparison of polymerization and damage power thresholds (P_{th} , D_{th}) for the triazole-based initiators and Irgacure369 (I369). No polymerization is indicated in gray, the polymerization window is marked green and damaging conditions are red. A,B) P_{th} and D_{th} in dependence of the photoinitiator concentration for PEGDA and PETA. C,D) P_{th} and D_{th} in dependence of the laser scanning speed at a constant photoinitiator concentration of 4×10^{-3} M.

In PETA polymerizations, the results obtained for **Me-Mono** and **Ph-Mono** were similar to those previously described with PEGDA (Figure 3A,B). Reductions in P_{th} of 20% and 14%, respectively, were observed when increasing the photoinitiator concentration from 0.8×10^{-3} M to 4×10^{-3} M and further reductions of 8% and 6%, respectively, were observed when the concentration was increased to 8×10^{-3} M. It is widely accepted that higher concentrations of polymerizable functional groups increase the reactivity of monomer solutions. Accordingly, PETA requires less energy to polymerize and features significantly lower damage thresholds for all photoinitiators. This results in smaller polymerization windows of around

half the magnitude of those obtained with PEGDA. Lower polymerization thresholds are favorable to enable high fabrication speeds for small feature sizes and also for photoresists that are susceptible to strong local heating and microexplosions (e.g., those containing metals).^[53] The aforementioned solubility issues associated with **Me-Bis** and **Ph-Bis** were considerably more pronounced in PETA; even at the lowest concentration of 0.8×10^{-3} M the resists were not fully homogeneous and poor results were obtained during microfabrication with these initiators (Figure 3D).

In general, it can be expected that increased scanning speeds lead to increased P_{th} 's due the reduced exposure dose of

photons. Indeed, this trend can be observed with both PEGDA and PETA for all photoinitiators (Figure 3C,D). Interestingly however, these effects were less pronounced in the resists containing the triazole-based initiators than in those containing **I369**. This was particularly evident with PEGDA, where the P_{th} increased by no more than 4–8% with each stepwise increase in scanning speed for the triazole-based initiators, while an increase of 18% was observed for **I369**. This demonstrates that the triazole-based initiators are more efficient than **I369**; requiring lower energy doses to achieve the same polymerization. Accordingly, the triazole-based initiators can enable microfabrication at higher scanning speeds, thus reducing the required fabrication time when compared to **I369**.

2.4. Micro-Raman Spectroscopic Analysis of Microstructures

To further evaluate the success of the triazole-based initiators in two-photon polymerization, micro-Raman spectroscopy was performed on the surface of the microfabricated cubes. From this analysis, the degree of consumption of vinyl groups (DC) from monomer to polymer was determined by measuring the change in the ratio of peak areas associated with the C=C ($\approx 1638\text{ cm}^{-1}$) and C=O ($\approx 1728\text{ cm}^{-1}$) bonds before and after polymerization, according to Equation (1)

$$DC = \left[1 - \left(\frac{A_{C=C}/A_{C=O}}{A'_{C=C}/A'_{C=O}} \right) \right] \times 100 \quad (1)$$

where $A_{C=C}$, $A_{C=O}$, $A'_{C=C}$, and $A'_{C=O}$ are the integrated intensities of Raman peaks related to the C=C and C=O moieties in the polymerized and the monomeric resins (Figure 5).^[54] Under this framework, it is assumed that the C=C bond order is reduced, i.e., to C–C, as a consequence of attachment of radicals to the C=C bonds of the monomer during polymerization and crosslinking, resulting in a decrease in the intensity of the C=C peak; as C=O bonds do not participate in these radical reactions, the intensity remains constant and therefore C=O acts as an internal reference. It is additionally assumed that the Michael addition transformation does not induce the disproportionation of C=C bonds; yet, as this process is likely, the determined DCs represent an estimate of the lower limit.^[55–57]

We were pleased to observe that the DCs in both PETA and PEGDA were either comparable or better when the triazole-based initiators **Me-Mono** and **Ph-Mono** were employed in comparison to those achieved with **I369**. In general, the DCs in PETA samples were broadly consistent with that observed previously,^[58] with the following order of effectiveness of the photoinitiators: **Ph-Mono** > **I369** > **Me-Mono**. The DC values in PETA are limited to a maximum achievable level of less than 50% due to the restricted mobility of the oligomers and the reduced structural flexibility in the 3D network that is produced on polymerization.^[58] Interestingly, the DCs in PEGDA samples (which can reach a maximum of 100%) followed the opposite trend in initiator efficiency: **Me-Mono** > **I369** > **Ph-Mono**, which is likely due to differences in solubility between the initiators in the two resins. The homogeneity of DC was also confirmed by spectroscopic mapping (Figure 4), where only 3% variation in DC (standard deviation as a function of the mean) was observed

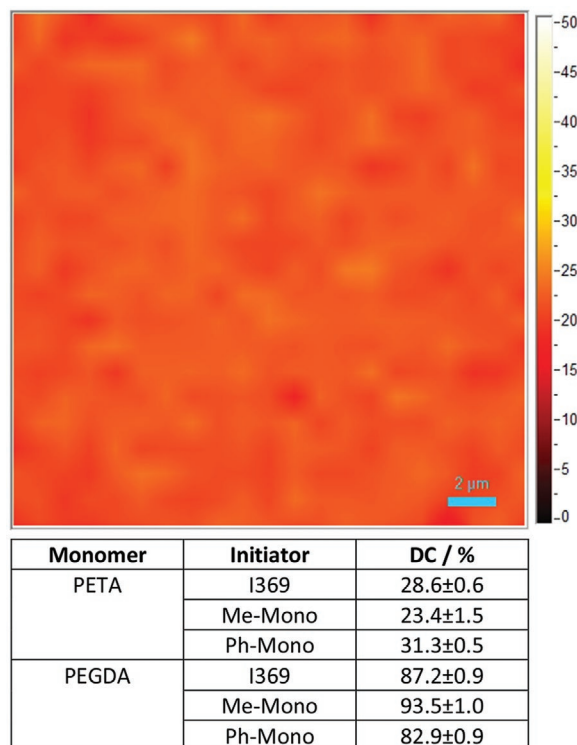


Figure 4. Micro-Raman spectroscopic analysis of the $5 \times 5 \times 5\ \mu\text{m}$ cubes microfabricated with $4 \times 10^{-3}\ \text{M}$ photoinitiator at $20\ \text{mm s}^{-1}$ applying a laser power of 18 mW for PETA and 27 mW for PEGDA. Top: Raman mapping of the DC confirms the homogeneity of monomer conversion; Bottom: DC in the printed structures ($N = 3$). To account for the strong overlap of peaks from the monomer/polymer and the photoinitiators, the spectra were fit with mixed Gaussian–Lorentzian peak shapes to enable accurate deconvolution and quantification of areas.

from 441 spectra collected from a $5 \times 5\ \mu\text{m}$ area. In summary, the micro-Raman spectroscopy demonstrates that comparable or even higher DCs can be achieved using the triazole-based initiators when compared to the reference compound **I369** and importantly these DCs were also shown to be uniform across the microfabricated structures.

2.5. Fabrication of Complex 3D Microarchitectures

To further evaluate the triazole-based initiators, the fabrication of more complex 3D microarchitectures was next investigated. Specifically, a series of bucky ball-type domes was produced (Figure 5). Optimal printing parameters were derived from the previously determined polymerization windows (Figure 3A). To allow for direct comparison of the microstructure quality, all photoresists were processed using the same scanning speed and laser power ($20\ \text{mm s}^{-1}$, 27 mW). **Me-Bis** and **Ph-Bis**, which were poorly soluble in PEGDA, resulted in collapsed 3D-structures after development (Figure 5B,C). Better results were obtained with **Me-Mono** and **Ph-Mono** (Figure 5D,E), which is consistent with their improved solubility and broader polymerization windows (Figure 3A). With **Ph-Mono** in particular, good structural integrity and comparable feature-resolution was

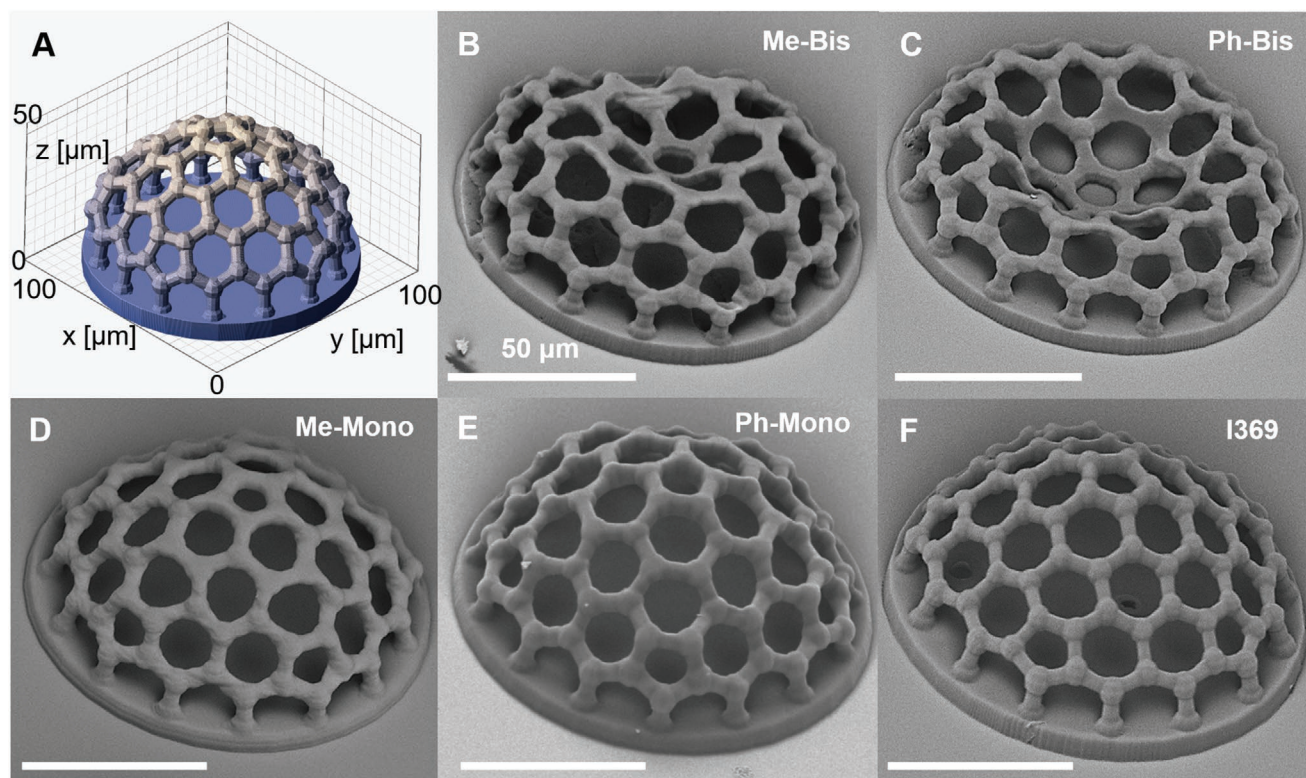


Figure 5. Scanning electron micrographs of microfabricated bucky ball-type domes. A) 3D design of bucky ball dome, B–F) Structures fabricated from PEGDA with 4×10^{-3} M photoinitiator at a 20 mm s^{-1} and a laser power of 27 mW.

observed in comparison to the reference initiator. This further demonstrates the quality of microstructures that be fabricated using triazole-based initiators.

3. Conclusion

It has been demonstrated that the copper catalyzed azide/alkyne cycloaddition (CuAAC) reaction can enable the synthesis of efficient photoinitiators for two-photon induced polymerization. This provides a new and robust method for the expedient synthesis of novel photoinitiators via a click chemistry strategy. In this study, four novel triazole-based initiators were synthesized using this approach and these compounds were characterized by one and two-photon spectroscopy. The triazole-based initiators were then shown to effectively induce two-photon polymerization of the common acrylate resins PETA and PEGDA. When compared to the commonly employed commercial initiator Irgacure369 (**I369**), the triazole-based initiators **Me-Mono** and **Ph-Mono** were shown to have comparable or higher sensitivity and to better tolerate microfabrication at increased scanning speeds. Finally, surface analysis of the fabricated microstructures by micro-Raman spectroscopy demonstrated that a high degree of consumption of vinyl groups and good homogeneity can be obtained using the triazole-based initiators. Due to the reliable and high-yielding nature of the CuAAC reaction, and the efficiency of the resulting photoinitiators, we are confident that this rapid and modular approach will find utility in the synthesis of new

photoinitiators for various applications related to microfabrication via two-photon polymerization.

4. Experimental Section

Representative Procedure for the Synthesis of Triazole-Based Initiators: 4,4'-(4,4'-(9,9-Dioctyl-9H-fluorene-2,7-diyl)bis(1H-1,2,3-triazole-4,1-diyl))bis(*N,N*-dimethylaniline) (**Me-Bis**)

The diyne **2** (100 mg, 0.228 mmol, 1.0 equiv.), 4-azido-*N,N*-dimethylaniline (**8**) (78 mg, 0.479 mmol, 2.1 equiv.) and TBTA (tris[1-benzyl-1H-1,2,3-triazol-4-yl)methyl]amine) (6.0 mg, 0.0114 mmol, 5 mol%) were combined and then dissolved in CH_2Cl_2 (10 mL). The solution was degassed with argon for 5 min before the addition of $\text{Cu}(\text{MeCN})_4\text{PF}_6$ (4.2 mg, 0.0114 mmol, 5 mol%). The reaction mixture was stirred for 18 h, concentrated under reduced pressure and then purified by silica gel column chromatography (eluting with 0–2% MeOH in CH_2Cl_2) to yield the title compound (168 mg, 0.220 mmol, 96%) as an off-white amorphous solid.

IR (neat)/ cm^{-1} : 2917, 2843, 1614, 1462, 1342; **¹H NMR** (400 MHz, CDCl_3) δ 7.97 (2H, app br d, *J* 1.0), 7.85 (2H, dd, *J* 7.8, 1.5), 7.78 (2H, app br d, *J* 7.9), 7.68–7.61 (4H, m), 6.84 (4H, d, *J* 8.6), 3.05 (12H, s), 2.15–2.03 (4H, m), 1.21–0.96 (20H, m), 0.77 (6H, t, *J* 7.0), 0.73–0.61 (4H, m); **¹³C NMR** (126 MHz, CDCl_3) δ 151.9, 150.8, 148.6, 141.0, 129.6, 127.0, 124.7, 122.2, 120.2 (2 resonances), 117.9, 112.5, 55.7, 40.7 (2 resonances), 31.9, 30.2, 29.4, 29.4, 24.0, 22.7, 14.2; **HRMS** (ESI) Calculated for $\text{C}_{49}\text{H}_{63}\text{N}_8$ [$\text{M}+\text{H}$] $^+$ 763.5170, found 763.5167.

Photophysical Measurements: One-photon UV–vis spectra were recorded on a Mettler Toledo UV5Bio spectrophotometer using 10 mm path length quartz cuvettes with concentrations $\approx 10^{-6}$ M in spectroscopic grade solvents. Steady state emission and excitation spectra were recorded on an Edinburgh Instruments FP920 Phosphorescence Lifetime Spectrometer equipped with a 450 W steady state xenon lamp and interchangeable EPL pulsed diode lasers excitation sources, and a red

sensitive photomultiplier in Peltier (air cooled) housing (Hamamatsu R928P). Lifetime data were recorded following excitation with an EPL laser using time correlated single photon counting. Fluorescence quantum yields were determined with an integrating sphere, using a solvent blank to establish the absorption. Lifetimes were determined using a reconvolution fit with the instrumental response function on the data obtained, and quality of fit judged by minimization of reduced χ -squared and residuals squared.

Two-photon absorption spectra were determined in the 700–750 nm range using the relative two-photon fluorescence method on 10^{-4} M toluene solution of the dyes in 10 mm quartz cuvettes.^[59] The samples were excited using a Spectra-Physics Mai Tai Ti:sapphire laser, 100 fs pulse width and 80 MHz repetition rate, focused onto the sample using a microscope objective (10 \times , NA 0.25); spectra were recorded using an Ocean Optics QE650000 compact CCD spectrometer. Two-photon absorption cross sections were calculated relative to rhodamine B^[60] in methanol using the equation

$$\delta_{\text{sam}} = \delta_{\text{ref}} \frac{\langle F_{\text{sam}} \rangle n_{\text{sam}}^2 C_{\text{ref}} \Phi_{\text{ref}} P_{\text{ref}}^2}{\langle F_{\text{ref}} \rangle n_{\text{ref}}^2 C_{\text{sam}} \Phi_{\text{sam}} P_{\text{sam}}^2} \quad (2)$$

Where *ref* and *sam* describe the reference and the sample, respectively; $\langle F \rangle$ is the average fluorescence intensity integrated from the two-photon fluorescence spectrum; *n* is the refractive index of the solvent; *C* is the concentration of the solution; Φ is the fluorescence quantum yield; and *P* is the laser power. The quadratic dependence of the luminescence intensity on the excitation power was checked for each sample at all wavelengths, indicating that the measurements were carried out in intensity regimes where saturation or photodegradation did not occur.

Two-Photon Polymerization: All microstructures were fabricated on a commercially available 2PP system (Nanoscribe Photonic Professional, GmbH, Germany). The set-up is equipped with a near infrared (NIR) fiber laser, a high-sensitivity microscope camera for real time observation of the printing process and an ultraprecise piezo mode for arbitrary 3D trajectories (FBMS) as well as the high-speed galvo mode (MBFS) for fast structuring in a layer-by-layer fashion. The laser features a center wavelength of 780 nm with a pulse repetition rate of 80 MHz and pulse duration of ≈ 100 fs. The laser beam was focused using a 63 \times microscope objective (Zeiss, NA 1.4 with oil immersion media) mounted on a linear stage for vertical positioning. All 3D structures were designed using the computer aided design software Spaceclaim (Ansys Inc) and printing parameters were set by the Describe software.

Sample Development: Glass coverslips (22 \times 22 mm², thickness *n*.1.5) served as the substrates for 2PP microstructures. They were first rinsed with acetone ($\geq 99.9\%$, Sigma-Aldrich) followed by isopropanol (IPA) (anhydrous 99.5% Sigma-Aldrich) and blow-dried with nitrogen. The coverslips were then fixed to the provided sample holders using sticky tape (Photonic Professional GT, Nanoscribe GmbH). A drop of immersion oil was applied on the bottom of the substrate and 40 μ L of photoresist were pipetted on the top side of the substrate.

Visualization of 2PP Structures: The bright field microscope Eclipse LV100ND (Nikon) with the NIS-Elements Imaging software was used to determine polymerization- and damage- thresholds with 20 \times and 50 \times objectives (Zeiss, NA 0.45 and NA 0.8).

Scanning electron microscopy (SEM) was used to obtain 3D images of the 2PP microstructures by tilting the sample 0 $^\circ$ –45 $^\circ$ and to resolve microscopic features. All samples were dried overnight and sputter coated with platinum to a nominal thickness of about 10 nm to provide a conducting layer for SEM imaging. They were imaged using a table-top SEM by Hitachi TM3030.

Micro-Raman Spectroscopy: Micro Raman spectroscopy and imaging was performed using a Horiba Jobin Yvon LabRAM HR Raman microscope equipped with an automated xyz stage (Märzhäuser). Spectra were acquired using a 785 nm laser at 24 mW power, a 100 \times objective and a 50 μ m confocal pinhole. To simultaneously scan a range of Raman shifts, a 300 lines mm⁻¹ rotatable diffraction grating

along a path length of 800 mm was employed. Spectra were detected using a Synapse CCD detector (1024 pixels) thermoelectrically cooled to -60 $^\circ$ C. Before spectra collection, the instrument was calibrated using the zero-order line and a standard Si (100) reference band at 520.7 cm⁻¹. The spectral resolution in this configuration is better than 1.7 cm⁻¹. For single point measurements, spectra were acquired over the range 100–4000 cm⁻¹ with an acquisition time of 15–120 seconds and 4 accumulations to automatically remove the spikes due to cosmic rays and improve the signal to noise ratio. Spectra were collected from at least three random locations and averaged to give a mean spectrum. For multispectral imaging, spectra were acquired over the range 800–2130 cm⁻¹ at 1 μ m steps within a square 20 \times 20 μ m (a total of 441 spectra). As each individual spectrum was collected for 60 s, repeated once, the whole map required ≈ 15 h of acquisition time. To calculate the degree of consumption of vinyl groups (DC), spectra were extracted within the range 1550–1800 cm⁻¹, baseline corrected using second-order polynomial fitting models and peaks deconvoluted using mixed Gaussian-Lorentzian (50:50) shapes.

Supporting Information

Supporting Information is available from the Wiley Online Library or from the author.

Acknowledgements

This research was supported by a University of Nottingham Interdisciplinary Centre for Analytical Science (UNICAS) award (I.H., B.P., and J.M.) and the Natural Environment Research Council (Grant No. NE/R011230/1) (A.W.). The authors would like to thank Dr. Louise Natrajan (UoM) and Prof. Robert Stockman (UoN) for access to equipment and for helpful discussions.

Conflict of Interest

The authors declare no conflict of interest.

Keywords

click chemistry, CuAAC, microfabrication, photoinitiators, two photon polymerization

Received: July 20, 2020
Revised: August 20, 2020
Published online:

- [1] H. J. Kong, S. W. Yi, D.-Y. Yang, K.-S. Lee, J.-B. Kim, T. Lim, S. Kim, in *Micromach. Technol. Micro-Optics Nano-Optics V Microfabr. Process Technol. XII*, Vol. 6462, Proc. SPIE, San Jose, CA 2007.
- [2] X. Zhou, Y. Hou, J. Lin, *AIP Adv.* **2015**, 5, 030701.
- [3] R. Luttge, *Nano- and Microfabrication For Industrial and Biomedical Applications*, 2nd ed., William Andrew Publishing, Boston, MA 2016, pp. 87–134.
- [4] M. Li, W. H. Li, J. Zhang, G. Alici, W. Wen, *J. Phys. D: Appl. Phys.* **2014**, 47, 063001.
- [5] K. S. Teh, *Front. Mech. Eng.* **2017**, 12, 490.
- [6] C. N. LaFratta, J. T. Fourkas, T. Baldacchini, R. A. Farrer, *Angew. Chem., Int. Ed.* **2007**, 46, 6238.
- [7] J. F. Xing, X. Z. Dong, W. Q. Chen, X. M. Duan, N. Takeyasu, T. Tanaka, S. Kawata, *Appl. Phys. Lett.* **2007**, 90, 131106.

- [8] Z. Li, N. Pucher, K. Cicha, J. Torgersen, S. C. Ligon, A. Ajami, W. Husinsky, A. Rosspeintner, E. Vauthey, S. Naumov, T. Scherzer, J. Stampfl, R. Liska, *Macromolecules* **2013**, *46*, 352.
- [9] (Eds. J. Lalevé, J.-P. Fouassier, *Photopolymerisation Initiating Systems*, Royal Society Of Chemistry, Cambridge, **2018**.
- [10] R. Whitby, Y. Ben-Tal, R. MacMillan, S. Janssens, S. Raymond, D. Clarke, J. Jin, A. Kay, M. C. Simpson, *RSC Adv.* **2017**, *7*, 13232.
- [11] T. Baldacchini, *Three-Dimensional Microfabrication Using Two-Photon Polymerization: Fundamentals, Technology and Applications*, Elsevier, **2015**.
- [12] H. C. Kolb, M. G. Finn, K. B. Sharpless, *Angew. Chem., Int. Ed.* **2001**, *40*, 2004.
- [13] G. A. Rance, W. A. Solomonsz, A. N. Khlobystov, *Chem. Commun.* **2013**, *49*, 1067.
- [14] J. E. Moses, A. D. Moorhouse, *Chem. Soc. Rev.* **2007**, *36*, 1249.
- [15] a) D. Brunel, F. Dumur, *New J. Chem.* **2020**, *44*, 3546; b) A. J. Maroulis, C. P. Hadjiantoniou-Maroulis, B. Georgiou, G. Seretoudi, I. Sideridou-Karayannidou, *J. Macromol. Sci. A* **1994**, *31*, 487; c) J. Wang, J. Mei, R. Hu, J. Z. Sun, A. Qin, B. Z. Tang, *J. Am. Chem. Soc.* **2012**, *134*, 9956; d) A. Qin, J. W. Y. Lam, L. Tang, C. K. W. Jim, H. Zhao, J. Sun, B. Z. Tang, *Macromolecules* **2009**, *42*, 1421; e) H. Liu, L. Wang, Y. Wu, Q. Liao, *RSC Adv.* **2017**, *7*, 19002.
- [16] J. B. Mueller, J. Fischer, F. Mayer, M. Kadic, M. Wegener, *Adv. Mater.* **2014**, *26*, 6566.
- [17] K. J. Schafer, J. M. Hales, M. Balu, K. D. Belfield, E. W. Van Stryland, D. J. Hagan, *J. Photochem. Photobiol. A Chem.* **2004**, *162*, 497.
- [18] K. D. Belfield, S. Yao, M. V. Bondar, in *Adv. Polym. Sci.*, **2008**, pp. 97–156.
- [19] C. D. Andrade, C. O. Yanez, L. Rodriguez, K. D. Belfield, *J. Org. Chem.* **2010**, *75*, 3975.
- [20] H. Zhang, J. Fan, H. Dong, S. Zhang, W. Xu, J. Wang, P. Gao, X. Peng, *J. Mater. Chem. B* **2013**, *1*, 5450.
- [21] T. Yang, Y. Zuo, Y. Zhang, Z. Gou, X. Wang, W. Lin, *J. Mater. Chem. B* **2019**, *7*, 4649.
- [22] K. D. Belfield, M. V. Bondar, C. O. Yanez, F. E. Hernandez, O. V. Przhonska, *J. Mater. Chem.* **2009**, *19*, 7498.
- [23] M. J. Aljaafreh, S. Prasad, M. S. AlSalhi, Z. A. Alahmed, M. M. Al-Mogren, *Polymers* **2019**, *11*, 1534.
- [24] K. D. Belfield, K. J. Schafer, Y. Liu, J. Liu, X. Ren, E. Van Stryland, *J. Phys. Org. Chem.* **2000**, *13*, 837.
- [25] I. Fitisilis, M. Fakis, I. Polyzos, V. Giannetas, P. Persephonis, *J. Photochem. Photobiol. A Chem.* **2010**, *215*, 25.
- [26] C. Katan, S. Tretiak, M. H. V. Werts, A. J. Bain, R. J. Marsh, N. Leonczek, N. Nicolaou, E. Badaeva, O. Mongin, M. Blanchard-Desce, *J. Phys. Chem. B* **2007**, *111*, 9468.
- [27] J.-Z. Cheng, C.-C. Lin, P.-T. Chou, A. Chaskar, K.-T. Wong, *Tetrahedron* **2011**, *67*, 734.
- [28] M. Tromayer, P. Gruber, A. Rosspeintner, A. Ajami, W. Husinsky, F. Plasser, L. González, E. Vauthey, A. Ovsianikov, R. Liska, *Sci. Rep.* **2018**, *8*, 17273.
- [29] S. Liu, K. Zhang, J. Lu, J. Zhang, H.-L. Yip, F. Huang, Y. Cao, *J. Am. Chem. Soc.* **2013**, *135*, 15326.
- [30] X. Peng, Q. Wang, Y. Mishra, J. Xu, D. E. Reichert, M. Malik, M. Taylor, R. R. Luedtke, R. H. Mach, *Bioorg. Med. Chem. Lett.* **2015**, *25*, 519.
- [31] W.-Y. Lee, T. Kurosawa, S.-T. Lin, T. Higashihara, M. Ueda, W.-C. Chen, *Chem. Mater.* **2011**, *23*, 4487.
- [32] V. V. Rostovtsev, L. G. Green, V. V. Fokin, K. B. Sharpless, *Angew. Chem., Int. Ed.* **2002**, *41*, 2596.
- [33] G. J. Kubas, B. Monzyk, A. L. Crumblis, *Inorg. Synth.* **1990**, *28*, 68.
- [34] T. R. Chan, R. Hilgraf, A. K. Barry Sharpless, V. V. Fokin, *Org. Lett.* **2004**, *6*, 2853.
- [35] M. A. Albota, C. Xu, W. W. Webb, *Appl. Opt.* **1998**, *37*, 7352.
- [36] A. R. Morales, A. Frazer, A. W. Woodward, H.-Y. Ahn-White, A. Fonari, P. Tongwa, T. Timofeeva, K. D. Belfield, *J. Org. Chem.* **2013**, *78*, 1014.
- [37] W. V. Moreshead, O. V. Przhonska, M. V. Bondar, A. D. Kachkovski, I. H. Nayyar, A. E. Masunov, A. W. Woodward, K. D. Belfield, *J. Phys. Chem. C* **2013**, *117*, 23133.
- [38] A. R. Ballestas-Barrientos, A. W. Woodward, W. V. Moreshead, M. V. Bondar, K. D. Belfield, *J. Phys. Chem. C* **2016**, *120*, 7829.
- [39] K. D. Belfield, K. J. Schafer, W. Mourad, B. A. Reinhardt, *J. Org. Chem.* **2000**, *65*, 4475.
- [40] J. M. Hales, D. J. Hagan, E. W. Van Stryland, K. J. Schafer, A. R. Morales, K. D. Belfield, P. Pacher, O. Kwon, E. Zojer, J. L. Bredas, *J. Chem. Phys.* **2004**, *121*, 3152.
- [41] M. Tromayer, P. Gruber, A. Rosspeintner, A. Ajami, W. Husinsky, F. Plasser, L. González, E. Vauthey, A. Ovsianikov, R. Liska, *Sci. Rep.* **2018**, *8*, 17273.
- [42] Z. Li, N. Pucher, K. Cicha, J. Torgersen, S. C. Ligon, A. Ajami, W. Husinsky, A. Rosspeintner, E. Vauthey, S. Naumov, T. Scherzer, J. Stampfl, R. Liska, *Macromolecules* **2013**, *46*, 352.
- [43] C. Li, L. Luo, S. Wang, W. Huang, Q. Gong, Y. Yang, S. Feng, *Chem. Phys. Lett.* **2001**, *340*, 444.
- [44] R. Nazir, E. Balčiūnas, D. Buczyńska, F. Bourquard, D. Kowalska, D. Gray, S. Maćkowski, M. Farsari, D. T. Gryko, *Macromolecules* **2015**, *48*, 2466.
- [45] A. K. Nguyen, S. D. Gittard, A. Koroleva, S. Schlie, A. Gaidukeviciute, B. N. Chichkov, R. J. Narayan, *Regener. Med.* **2013**, *8*, 725.
- [46] A. Ovsianikov, M. Malinauskas, S. Schlie, B. Chichkov, S. Gittard, R. Narayan, M. Löbner, K. Sternberg, K. P. Schmitz, A. Haverich, *Acta Biomater.* **2011**, *7*, 967.
- [47] It should be noted that several of the D's exceeded the maximum laser power applied (LPmax ≈ 40 mW).
- [48] This was often in the form of macroscopic clusters rather than fully polymerized structures due to the poor mechanical stability and shrinkage observed at threshold power.
- [49] S. Krivec, N. Matsko, V. Satzinger, N. Pucher, N. Galler, T. Koch, V. Schmidt, W. Grogger, R. Liska, H. C. Lichtenegger, *Adv. Funct. Mater.* **2010**, *20*, 811.
- [50] C. Martineau, R. Anémian, C. Andraud, I. Wang, M. Bouriau, P. L. Baldeck, *Chem. Phys. Lett.* **2002**, *362*, 291.
- [51] Z. Li, J. Torgersen, A. Ajami, S. Mühleder, X. Qin, W. Husinsky, W. Holthöner, A. Ovsianikov, J. Stampfl, R. Liska, *RSC Adv.* **2013**, *3*, 15939.
- [52] Specifically, via micro-explosions that become evident in damaged structures.
- [53] L. Vurth, P. Baldeck, O. Stéphane, G. Vitrant, *Appl. Phys. Lett.* **2008**, *92*, 171103.
- [54] R. Houbertz, G. Domann, J. Schulz, B. Olsowski, L. Fröhlich, W.-S. Kim, *Appl. Phys. Lett.* **2004**, *84*, 1105.
- [55] F. Burmeister, S. Steenhusen, R. Houbertz, U. D. Zeitner, S. Nolte, A. Tünnermann, *J. Laser Appl.* **2012**, *24*, 042014.
- [56] Y. Liu, Q. Hu, F. Zhang, C. Tuck, D. Irvine, R. Hague, Y. He, M. Simonelli, G. Rance, E. Smith, R. D. Wildman, *Polymers* **2016**, *8*, 325.
- [57] Q. Hu, X.-Z. Sun, C. D. J. Parmenter, M. W. Fay, E. F. Smith, G. A. Rance, Y. He, F. Zhang, Y. Liu, D. Irvine, C. Tuck, R. Hague, R. Wildman, *Sci. Rep.* **2017**, *7*, 17150.
- [58] L. J. Jiang, Y. S. Zhou, W. Xiong, Y. Gao, X. Huang, L. Jiang, T. Baldacchini, J.-F. Silvain, Y. F. Lu, *Opt. Lett.* **2014**, *39*, 3034.
- [59] C. Xu, W. W. Webb, *J. Opt. Soc. Am. B* **1996**, *13*, 481.
- [60] N. S. Makarov, M. Drobizhev, A. Rebane, *Opt. Express* **2008**, *16*, 4029.